Electrochimica Acta 353 (2020) 136493

Contents lists available at ScienceDirect

Electrochimica Acta

journal homepage: www.elsevier.com/locate/electacta

Morphology evolution and dendrite growth in Li- and Mg-metal batteries: A potential dependent thermodynamic and kinetic multiscale ab initio study

Arthur Hagopian [a, b], Drejc Kopač [c], Jean-Sébastien Filhol [a, b], Anja Kopač Lautar [c, *]

[a] Institut Charles Gerhardt, Université de Montpellier, CNRS, ENSCM, Montpellier, France
[b] RS2E French Network on Electrochemical Energy Storage, FR5439, Amiens, France
[c] National Institute of Chemistry, Ljubljana, Slovenia

ARTICLE INFO

Article history:
Received 14 February 2020
Received in revised form
8 May 2020
Accepted 17 May 2020
Available online 29 May 2020

Keywords:
Potential-dependent dendrite growth
DFT
kMC
Mg-metal batteries
Li-metal batteries
Multiscale modeling

ABSTRACT

It is well accepted that dendrites grow on anode surface of lithium-metal based batteries, while magnesium-metal batteries do not exhibit such a behavior. However, it has been recently shown experimentally and theoretically that magnesium can form uneven deposits that lead to similar safety concerns as lithium dendrites. To investigate a complex phenomenon such as dendritic growth from a theoretical point of view, it is necessary to study it on a multiscale level, i.e. from atomistic to meso scale. Herein we investigate thermodynamics, kinetics and morphology evolution of magnesium and lithium surfaces using density functional theory (DFT) and kinetic Monte Carlo (kMC) simulations. To be realistic for a device such as a battery, the electrochemical dimension has also to be included: this study was done within the framework of Grand canonical DFT approach that enables potential dependent DFT calculations, simulating relevant battery operating conditions. The atomistic potential dependent DFT results were upscaled using kMC simulations allowing to extract mesoscopic behavior at various operating potentials. The results of these calculations demonstrate the effect of potential on both the energetics and the dynamics of diffusion at the electrode-electrolyte interface. In particular, the equilibrium morphology of the metal electrode is strongly modified by the potential, leading to the stabilization of different surface orientations with potential. We show that the applied potential impacts atomic diffusion barriers leading to different surface mesoscopic relaxation times in the overall kinetics. The obtained results provide not only potential dependent information about systems morphology evolution, but also demonstrate the importance of using a suitable potential range (i.e. coherent with the experimental conditions): an unrealistic potential could lead to a very different behavior of the system on atomic and on meso scale.

1. Introduction

The increasing energy demand and consumption in the last decades, global warming and climate change resulted in energy research fields gaining a lot of attention and support. The fossil-free energy solutions are being investigated through various approaches, one of the main being the development of improved battery systems. Currently, Li-ion batteries are the most commonly used batteries in our everyday life. Nevertheless, to meet the energy requirements for the next decades, the current energy density of batteries should strongly increase [1–3]. Using Li-metal as the anode is one of the ways of achieving this goal. However, the tendency of lithium towards dendrite formation poses serious safety issues, and is hindering the development of a high energy density Li-metal battery technology [4]. One way of tackling this problem is the use of additives or the application of suitable protective films on Li-metal anode that would hinder dendrite growth [5]. Another approach is the development of the alternative battery architectures, and post-lithium batteries are gaining a lot of attention. Among the post-lithium battery candidates, Mg-metal battery represents one of the most interesting and promising architectures due to high volumetric and specific energy density (3833 mAh/cm^3 and 2205 mAh/g, respectively) [6–9]. It has been well accepted that

* Corresponding author.
E-mail address: anja.kopac.lautar@ki.si (A. Kopač Lautar).

https://doi.org/10.1016/j.electacta.2020.136493
0013-4686/

magnesium-metal batteries are less prone to dendrite formation, but are more inclined towards growth of smooth surfaces [10–15]. The safety issue posed by Li-metal batteries is therefore strongly reduced, and Mg-metal batteries development largely relies on the possibility of safely utilizing their respective metal anode. However, recent experimental [16–18] and theoretical [19] work has shown that dendrite growth, or uneven deposition, is not completely excluded in Mg-metal batteries. Therefore, more detailed understanding of the processes underlying the dendritic growth at these interfaces is needed to help develop a safe metal-battery technology.

It has been proposed that the self-diffusion barriers can serve as a descriptor for the dendrite growth [11,12]. Low diffusion barriers lead to fast diffusion that could facilitate smoothing the rough surface and contributes to dendrite-free surfaces. In opposite, high diffusion barrier results in slow diffusion and in the formation of isolated aggregates of adatoms that can serve as nucleus for dendrite growth [20,21]. In our previous work, this concept has been extended and linked to adsorption energies, lateral interaction energies, *k*-rates, and relaxation times [19]. Most of the theoretical work takes into account only the most stable surface. However, we have shown that in general the most stable surface is not always the dominant one, i.e. the one with the highest area fraction. This is due to the fact that the equilibrium shape of the crystal is determined by the surface energies, but also by the geometric orientation constraints as shown in the classical the Wulff construction [22]. The results we have obtained for the example of Mg system shows that the most stable surface is Mg(0001) with area fraction of 22.5% and 0.02 eV diffusion barrier, but the most commonly present surface is Mg($10\bar{1}1$) with area fraction of 49.5% and 0.29 eV diffusion barrier [19]. In comparison, Li(100) surface is the most stable surface orientation and has the highest area fraction in equilibrium shape of Li crystal (25–27%) [23–25]. The diffusion barrier on Li(100) is 0.14 eV [12], which is still only half as high as diffusion barrier on Mg($10\bar{1}1$). This demonstrates that if all experimentally commonly present Mg surfaces are taken into account and if self-diffusion barriers can indeed be seen as a descriptor for dendrite growth, then Mg could form dendrites. However, in our previous study the potential dependence of energetics and kinetics was not taken into account, and to the best of our knowledge, such a study has not yet been done. This is probably due to the fact that there is no widely accepted methodology that would allow potential dependent density functional (DFT) calculations. A very informative and relevant study investigating the influence of electric field on self-diffusion barriers was done recently [10]. However, the authors could not relate the electric field strength to the electrode potential.

Herein, we adopt Grand canonical DFT approach that uses the homogeneous background method to include the potential dependence into DFT calculations, as described in previous work [26–31]. This allows extraction of atomistic potential dependent energy parameters as well as the potential dependent energy barrier for diffusion steps of adatoms. A kinetic Monte Carlo (kMC) approach accounting for the potential dependent parameters is then used to obtain mesoscopic time scale and extended space scale. We have focused the study on three most commonly present Mg surfaces (Mg(0001), Mg($10\bar{1}0$), and Mg($10\bar{1}1$)) and two most commonly present Li surfaces (Li(100) and Li(110)). For both Mg and Li surfaces, we obtain potential dependent surface energies, adsorption and lateral interaction energies, diffusion barriers, *k*-rates, relaxation times, as well as area fractions and shape of the crystal. All of this information provides new and important insights into how potential governs the change in energetics, dynamics, and relaxation of a system. Importantly, the study demonstrates that taking potential into account provides results that differ from the ones obtained from neutral system, i.e. at potential of zero charge (PZC) which is usually the only one studied. Therefore, the results show that the potential should be precisely defined, as the energetics and dynamics of the system depend on the potential range studied.

The study of potential dependent morphology evolution presented herein offers a way to go beyond the atomic scale and static 0 K calculations limitation, and to obtain the kinetics and long time scale relaxation for the interface structuration. The presented methodology is general and allows investigation of complex interfaces under applied potential at DFT level and upscaling of the results. This methodology could be applied to investigate much more complex problems (yet at a higher computational cost) such as battery ageing, solvent degradation, solid electrolyte interphase (SEI) formation, or even be used to extract electrokinetic parameters giving the surface power generated by the electrochemical reaction: this would be of high value to evaluate the battery charge rate or the maximum power it can produce.

2. Computational details and theoretical methods

DFT calculations were performed using Vienna *Ab Initio* Simulation Package (VASP) [32,33]. The cutoff energy was set to 450 eV for both Mg and Li system, and the core electrons were described with projector augmented wave method (PAW) as implemented in VASP [34]. Generalized gradient approximation (GGA) and the functional of Perdew, Burke and Ernzerhof (PBE) were used to account for the exchange and correlation effects [35]. Electronic convergence criterion was set to 10^{-4} eV and force criterion to 0.01 eV/Å. In the NEB calculations, the convergence criterion was increased to 10^{-6} eV. For magnesium, Mg(0001), Mg($10\bar{1}0$) and Mg($10\bar{1}1$) were modeled using (4 x 4), (4 x 10) and (5 x 5) lattices, respectively. For lithium, both Li(100) and Li(110) surfaces were modeled using (3 x 3) lattices. In all cases, the lattice size was chosen so to prevent the periodic image interaction in order to reduce errors in the calculated adsorption and lateral interaction energies, as well as diffusion barriers, *k*-rates, and relaxation times (see S0 for more details). Mg and Li supercells structures, and a schematic representation of the adsorption energy E_{ads}, lateral interaction energy E_{int}, and diffusion barrier E_{diff} are presented in Supplementary information (Figs. S1, S2). In all calculations, a 5 and 7 layers symmetric slab was used to model Mg and Li surface, respectively. Bottom and upper layers were allowed to relax, while the middle layer was kept frozen to reduce interaction through strain of the two slab surfaces. For integration over the Brillouin zone, (5 x 5 x 1), (7 x 5 x 1), and (3 x 3 x 1) *k*-point meshes were used for Mg(0001), Mg($10\bar{1}0$), and Mg($10\bar{1}1$), respectively. For Li(100) and Li(110), (4 x 4 x 1) and (5 x 5 x 1) were used, respectively. The larger mesh in k-space always corresponds to the smallest lattice parameter in real space. To prevent interaction between periodic images in the z-direction, a vacuum of 30 Å was inserted between the Mg slabs and 15 Å between the Li slabs. The surrounding environment was described with implicit solvent by using the Polarizable Continuum Model (PCM) as implemented in VASPSol [36,37]. The dielectric constant ε that was used in calculations is the experimental value for common Mg and Li electrolytes, i.e. glyme-based ($\varepsilon = 7.2$) and ethylene-carbonate-based electrolytes ($\varepsilon = 89.9$), respectively.

Surface energy $E_{surface}$ is obtained using Eq. (1):

$$E_{surface} = (E_{slab} - E_{bulk}N_{slab})/(2A) \quad (1)$$

where E_{slab} is the calculated slab energy, E_{bulk} the energy of atom in the bulk, N_{slab} the number of atoms in the slab, and A the surface area. The surface energies determine the stability of a specific

surface orientation. Thus, the calculated surface energies are used in constructing the equilibrium shape of the crystal with Wulff construction, which is based on constrained energy minimization arguments (Fig. 1) [22]. Wulff constructions and surface area were obtained using VESTA [38].

The bonding strength of an adatom on a surface, i.e. its adsorption energy, depends on the surface orientation and on the adatom position on a specific surface. Only adsorption energies for the most favorable adsorption position for each surface are presented herein (Fig. 2), whereas the entire potential energy surfaces (PESs) are given in the Supplementary information (S1, Figs. S3a and S4a). Adsorption energy E_{ads} was calculated using Eq. (2):

$$E_{ads} = E_{system} - E_{slab} - E_{atom}, \quad (2)$$

where E_{atom} is the energy of an isolated atom, and E_{system} is the energy of the slab with one adatom. Note that herein with this definition all the computed adsorption energies have negative value, and adsorption is the strongest for the most negative adsorption energy.

The diffusion rate of an adatom from one favorable adsorption site to the neighboring one depends on the energy barrier between the two sites. These energy diffusion barriers were calculated using nudged elastic band method (NEB) to determine minimum energy path (MEP) [39]. Although surface diffusion can occur via hopping or exchange mechanism, it has been shown that the exchange mechanism for smooth close packed surfaces is far less common [19]. The diffusion barriers for exchange mechanism can be more than an order of magnitude higher than for hopping mechanism. In nucleation theory of growth the *k*-rate follows the Arrhenius equation (Eq. (3)) [40].

$$k = \nu \exp\left(- E_{diff} \Big/ (k_b T)\right) \quad (3)$$

the diffusion barrier dependency is exponential, thus the exchange mechanism can be neglected.

Lateral interaction energy E_{int} was calculated using Eq. (4):

$$E_{int} = E_{system,2} - E_{slab} - 2E_{atom} - 2E_{ads}, \quad (4)$$

where $E_{system,2}$ is the energy of the slab with two neighbor adatoms. Lateral interaction energies between two neighboring adatoms are the essential part for constructing the cluster expansion in the kMC simulations. Since the lateral interaction energies are negative (i.e. the adatoms attract each other), the system will eventually form packed morphologies on the lattice at some characteristic time, defined herein as the relaxation time. Depending on the surface geometry and PES, the morphologies represent either islands or

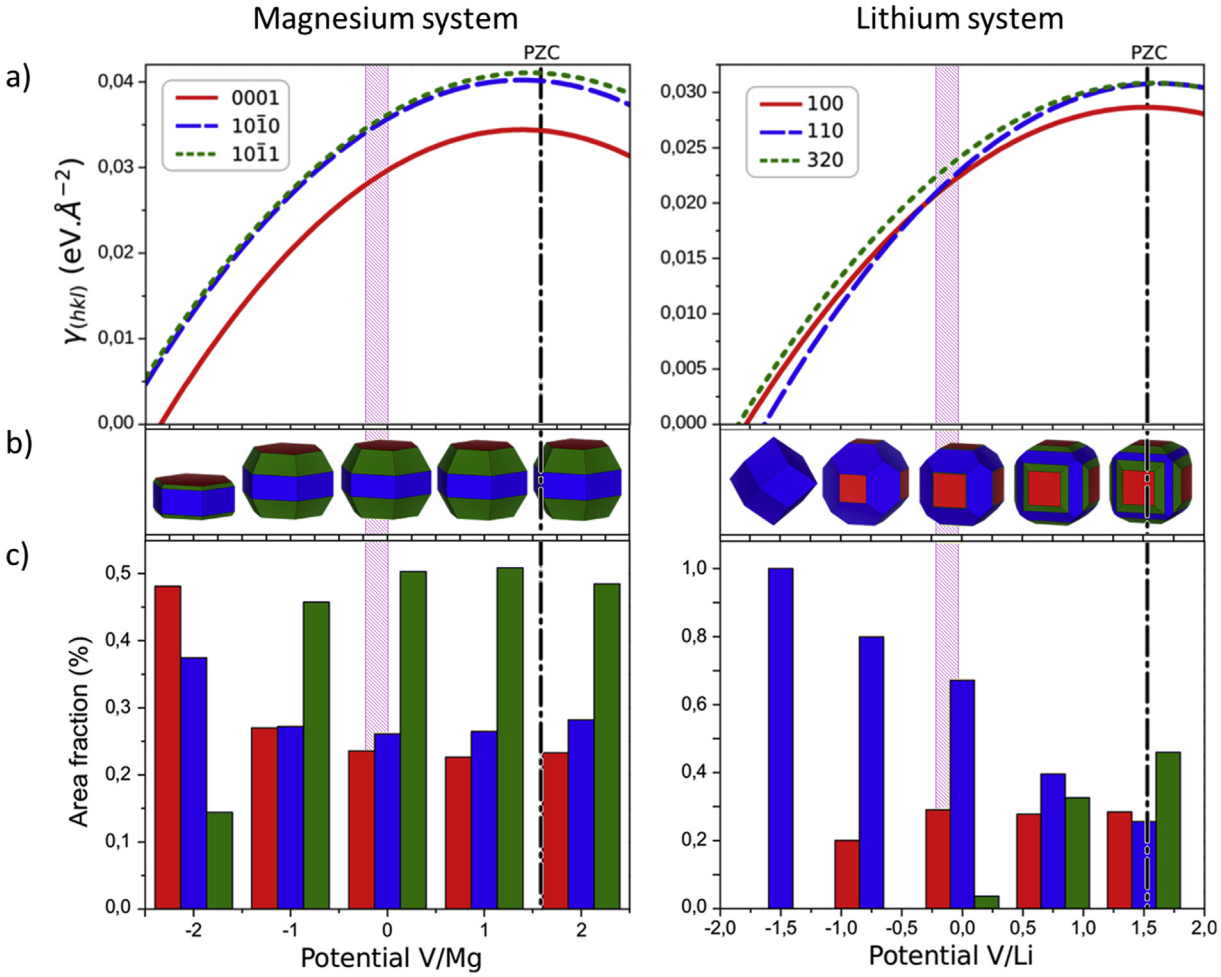

Fig. 1. Potential dependent (a) surface tension, (b) equilibrium shape of the crystal as obtained with Wulff construction, and (c) area fraction of specific surface orientation for (left) magnesium and (right) lithium system. In both systems, the studied surface orientations are marked with red, blue and green, from most stable surface studied to the least stable one at PZC. The averaged value of the PZC is marked with black line at 1.58 V/Mg and 1.52 V/Li. The pink shaded region marks the standard working battery regime (from −0.2 V/Mg to 0 V/Mg, and from −0.2 V/Li to 0 V/Li). (For interpretation of the references to colour in this figure legend, the reader is referred to the Web version of this article.)

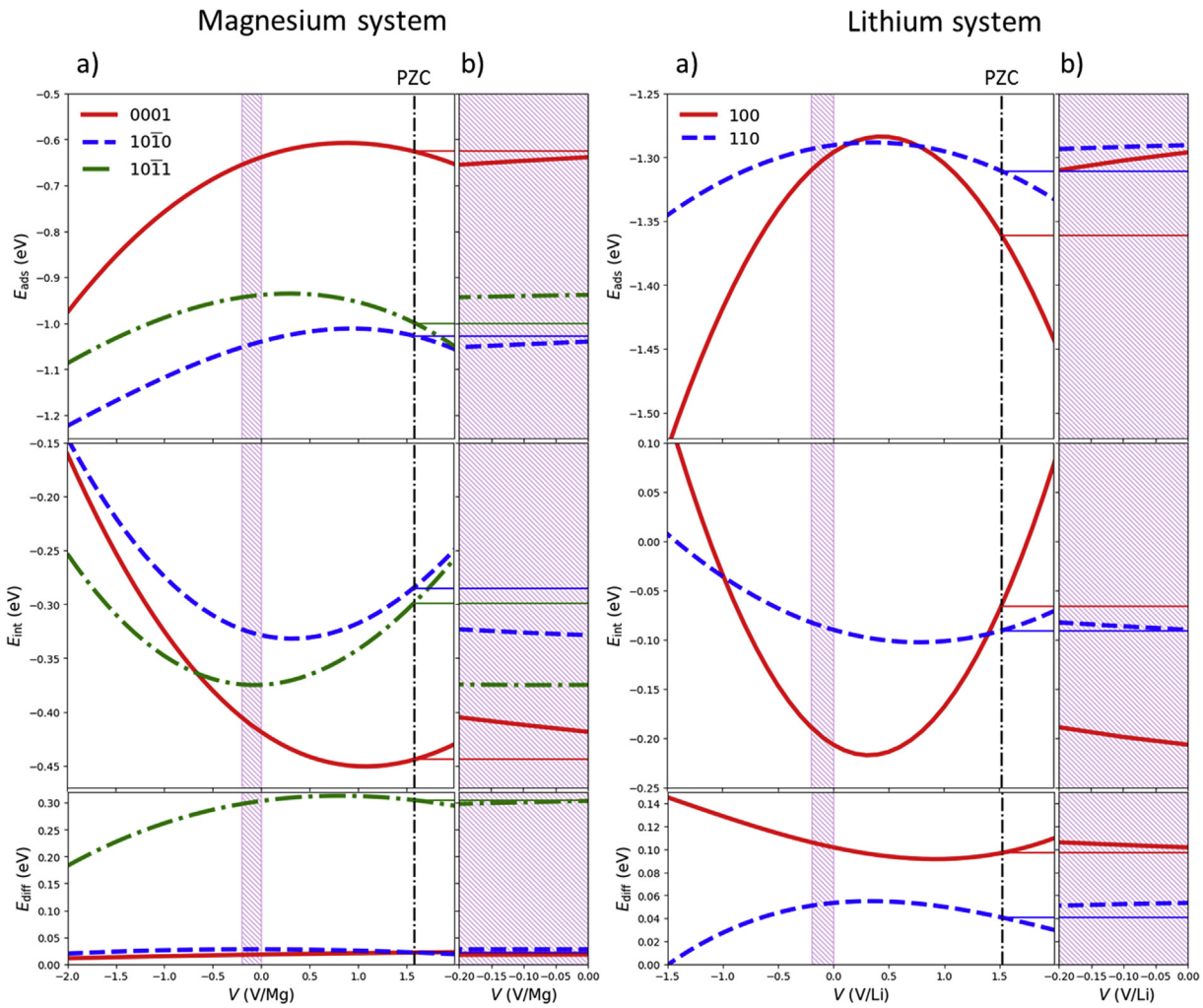

Fig. 2. Potential dependence of (top) adsorption energy, (middle) lateral interaction energy, and (bottom) diffusion barrier for (left) Mg and (right) Li system. (a) Graphs plotted in a wide potential range. Standard working battery regime is marked with pink shaded region, whereas potential of zero charge (1.58 V/Mg and 1.52 V/Li) is marked with black line. (b) Potential dependent adsorption and lateral interaction energies and diffusion barriers at standard working battery regime. Solid horizontal red, blue and green line represent values of adsorption and interaction energies, and diffusion barriers at PZC for Mg(0001), Mg(10$\bar{1}$0), and Mg(10$\bar{1}$1), respectively, in Mg system, and for Li(100) and Li(110) in Li system. (For interpretation of the references to colour in this figure legend, the reader is referred to the Web version of this article.)

continuous lines (Figs. S3c and S4c). After the relaxation time is reached, the sizes of islands or lines do not change for a significant time, which is much larger than a characteristic timescale of surface reactions (inverse of the *k*-rates). The total energy of the system (the sum of E_{ads} for each atom and E_{int} for pairwise lateral interaction) reaches its local minimum at that time.

To assess the surface dynamics and study the timescale at which the system becomes relaxed, kMC simulations were used. Although various methods are available for performing kMC simulations [41,42], we used graph-theoretical kMC algorithm as implemented in the Zacros package (see S3 for more details) [43,44]. Simulations were done in a similar way as in our previous work [19], with the difference that here we ran each simulation at different potentials. The energetics, namely Mg or Li adatom adsorption energies, lateral interaction energies, and diffusion (via hopping) energy barriers were obtained from DFT, and are all potential dependent. Only first nearest neighbor adsorbate-adsorbate lateral interactions were included in the model, since the interactions with the second nearest neighbor is negligible (order of $E_{int} \approx 0.01$ eV). The energies used in the kMC model at various potentials for 3 different Mg surfaces and two different Li surfaces were obtained from Fig. 2. The *k*-rates for the kMC simulations assume a constant prefactor of $\nu = 10^{12}$ s^{-1}. The adsorption/desorption was not simulated, but instead the initial state was randomly distributed with adatoms, with 25% surface coverage. Since the coverage was the same for all surfaces, the relaxation timescales can be compared relatively between each other.

All of the above-mentioned calculations were done at various surface potentials. To vary the potential, we have used the grand canonical DFT approach discussed in detail in previous work [26–31]. In this approach the potential is varied by changing the charge of the unit cell, i.e. adding or subtracting electrons from the neutral system. The added/subtracted charge is neutralized by the homogeneous background of the exactly opposite charge. Difference between the Fermi energy of the system and the vacuum potential is defined as the potential of the system. Some general details of the grand canonical DFT approach are given in the Supplementary Information (S2) and in ref[30]. As we are in the grand potential framework, the relevant energy for further work and analysis is the so called free electrochemical energy *F(V)*. Free electrochemical energy *F(V)* and surface tension γ are closely connected through relation:

$$\gamma = F(V)/A \quad (5)$$

We will mostly refer to the free electrochemical energy in the remaining of the article, but as for all calculations for a specific surface the same surface area A was used, it can be seen from Eq. (5) that free electrochemical energy and surface tension can easily be interchanged. Expectedly, free electrochemical energy has similar potential dependence as the surface tension, a shape resembling an inverted parabola. To suitably describe the slight asymmetry of the potential dependence, all the potential dependent energetics were fitted with a third order polynomial. Note here that we will keep the terminology such as »surface energy«, »adsorption energy«, etc., but all these energies were computed in the grand canonical framework.

3. Results and discussion

3.1. Potential dependent surface energies and shape of the crystal

We study Mg and Li systems: three most commonly present Mg surfaces (Mg(0001), Mg($10\bar{1}0$), and Mg($10\bar{1}1$)) and two most commonly present Li surfaces: Li(100) and Li(110). For Mg system, the calculated potential of the neutral Mg system, i.e. Mg potential of zero charge (PZC) is 1.6 V/Mg, 1.5 V/Mg, and 1.64 V/Mg for Mg(), Mg($10\bar{1}0$), and Mg($10\bar{1}1$), respectively. On graphs, PZC is marked with an averaged value over the different surfaces of 1.58 V/Mg. In lithium case, we see that at least three surfaces are present on Wulff shape while considering uncharged surfaces (PZC): the herein studied Li(100) and Li(110), and additionally a stepped surface Li(320) (Fig. 1). The area fraction of Li(320) surface decreases with decreasing potential, and is no longer present on the Wulff shape for potentials lower than 0 V/Li. Thus, in the present work we focus only on the Li(100) and Li(110) surface. The calculated potential of zero charge for Li(100) and Li(110) is 1.53 V/Li and 1.69 V/Li, respectively. We plot the averaged value of 1.52 V/Li in the graphs.

We emphasize that the potential value of PZC is very far from the experimental domain, as the stripping/deposition should occur close to standard electrode potential. For example, the deposition of Mg^{2+} in Mg-metal batteries should preferably occur with an overpotential no larger than 200 mV [45]. We will refer to this potential (i.e. −0.2 V/Mg (V/Li) to 0 V/Mg (V/Li)) as the standard working battery regime. Nevertheless, under some conditions, in particular the ones leading to dendrites growth, larger overpotential up to 1 V can occur [46]. It is then important to understand how the potential shift can modify the morphology of the electrode and kinetic of the different elementary steps. To the best of our knowledge, potential dependent equilibrium shape of the crystal, adsorption and lateral interaction energies, diffusion barriers and k-rates were never investigated. Thus, we study a wide potential range for theoretical interest and information. Especially informative is the comparison of the energetics and dynamics of the system at the standard working battery regime with the neutral system that is usually studied in DFT calculations, i.e. the system at potential of zero charge (PZC).

The shape of the Mg crystal is not affected drastically by the applied potential. The area fractions remain approximately constant, leading only to small changes in the crystal appearance, and the crystal shape being a hexagon in a wide range of potential (Fig. 1). Only at extremely low potentials (−2 V/Mg) the area fraction of previously most common Mg($10\bar{1}1$) surface drastically decreases in favor of Mg($10\bar{1}0$) and Mg(0001). This results in a crystal obtaining a hexagonal platelet shape. Both hexagonal and hexagonal platelet shaped crystals of Mg were observed experimentally under reductive conditions [19], confirming the validity of our theoretical electrochemical approach. In contrast to Mg, the shape of Li crystal is considerably more potential dependent (Fig. 1). With decreasing potential, the area fraction of Li(110) is rapidly increasing, while the Li(100) decreases. At extremely low potential (−1.5 V/Li) Li(100) also disappears and the Li crystal structure obtains a rhombic dodecahedron geometry defined only by Li(110) surface. These shapes were also observed experimentally and serve as validation of this theoretical approach [47].

Worth emphasizing is that the information about battery operation at its standard working regime is the one gathered in the narrow region bellow the standard electrochemical potential of the studied system, and not around its potential of zero charge. The PZC is by almost 1.6 V and 1.5 V higher than the standard electrochemical potential in the case of Mg and Li, respectively. This means that any metallic Mg or Li particle is necessarily negatively charged. An uncharged metallic Mg or Li particle, i.e. the neutral systems as usually computed, correspond to potentials where Li or Mg metal is not stable and should oxidize to the corresponding cation. This means that studying dependence of energetics and kinetics at PZC, or at a random potential region, does not provide information about battery operation at its standard working regime. Surface potential/charge pair has to be carefully set in order to model the operating experimental conditions. The negative surface charge in the stability region is a direct consequence of the very low electronegativity of Mg and Li.

3.2. Potential dependent adsorption and lateral interaction energies, and diffusion barriers

Adsorption and lateral interaction energies have an effect on the morphology evolution of a surface. The general assumption is that diffusion is hindered when the adatoms are strongly adsorbed on the surface. This assumption is not valid in all cases, as seen in our results (vide infra). Slow diffusion and low lateral interactions lead to isolated adatom aggregates, which in nucleation theory of growth serve as a nucleus for further dendrite growth [20,21,40]. In contrast, adatoms experiencing weak adsorption energy and strong interaction will move more easily, which should result in epitaxial growth and smooth surfaces.

Calculated adsorption and interaction energy for Mg and Li system in a wide potential range both reveal parabolic (more precisely, third order polynomial) behavior (Fig. 2). Note that lower (more negative) energies represent stronger adsorption/interaction. Parabolic behavior of E_{ads} and E_{int} is not surprising, as potential dependence of surface energetics is closely linked to the surface tension (Eqs. (1), (2) and (4), and 5). The curvature of the energetics vs. potential (F–V) plot is directly linked to the differential capacitance C of the system [29].

$$C = \frac{-1}{A}\frac{\partial^2 F(V)}{\partial V^2} \quad (6)$$

Free energy can be approximated at second order by:

$$F = E(PZC) - \frac{1}{2}(V - PZC)^2 + \acute{O} \quad (7)$$

where E(PZC) is the energy at the potential of zero charge PZC, and ơ is residue due to not taking into account the asymmetry of potential dependence of energetics. The fact that adsorption and interaction energies are not linearly dependent on the potential reveals that the systems, from which the E_{ads} and E_{int} are calculated (Eqs. 2 and 4), have different differential capacitance. For example, potential dependence of adsorption energy results from the difference between calculated slab energy and calculated energy of

the slab with one adatom (Eq. (2)). Thus, surface with one adsorbed adatom has different capacitance than the initial smooth surface, more precisely about a percent higher capacitance than the smooth surface without any adatoms. This is expected, as a rough surface can hold more charge because of the larger atomic corrugation, i.e. it has higher differential capacitance.

Charging the system is equivalent to changing the potential: adding (subtracting) electrons corresponds to lowering (increasing) the potential, respectively. Charging of the system (in positive or negative direction) decreases the adsorption energy (increases its absolute value, i.e. adsorption energy is stronger and the adatoms are more strongly adsorbed) as it is energetically favorable to have rough surface (more adatoms). Rough surface has bigger surface area in comparison to smooth surface, which allows the increased surface charge to spread, i.e. to decrease the charge-charge repulsion on the surface thus increasing the capacitance. The consequence is that at a high potential (far away from PZC), the favored system is the one with the highest corrugation in order to reduce the charge-charge interaction. Atomic adsorption on a smooth surface increases roughness and is therefore favored. Thus, adsorption energy is decreasing (increasing in absolute value, i.e. stronger adsorption) for high reductive potentials as seen in Fig. 2 for all considered surfaces. In opposite, the dimerization of two atoms initially separated on a surface leads to reduction of the corrugation and is disfavored at low potential leading to increasing interaction energies (weaker interaction) (Fig. 2). Nevertheless, in the domain close to PZC, capacitive effects are not dominant and no simple rule can be easily given. Note that the top of parabola of E_{ads} and E_{int} is shifted in regard to PZC of smooth surface, whereas the energy of the smooth surface always has the top of its $F-V$ parabola at PZC (Figs. 1a and 2). The reason for this is that the PZC of the surface with added adatoms is shifted to lower potentials by about 100 meV per added adatom, depending on the atomic surface configuration, resulting in the PZC of E_{ads} and E_{int} is shifted as well (Eq. (7)). This can be explained by the reorganization of electron charge density upon addition of adatoms to the surface that change the surface dipole that is directly linked with PZC [27,48].

For Mg system the adsorption and interaction energies change the most with applied potential for Mg(0001), while they change approximately the same for Mg(10$\bar{1}$0) and Mg(10$\bar{1}$1). This can be understood by looking at their PES (Fig. S3a). The Mg(0001) surface is the most closely packed Mg surface, i.e. the most smooth one, whilst the atomic configuration of both Mg(10$\bar{1}$0) and Mg(10$\bar{1}$1) forms surface grooves. Thus, one adatom on the Mg(0001) surface has six possible neighboring adatoms, while one adatom one Mg(10$\bar{1}$0) or Mg(10$\bar{1}$1) has only two possible neighboring adatoms. Consequently, one adatom on Mg(0001) roughness the initially smooth surface to a larger extent than one adatom on Mg(10$\bar{1}$0) or Mg(10$\bar{1}$1). As discussed before, with the charging of the surface, the surface roughness is favored by strongly adsorbed and weakly interacting adatoms, explaining the stronger potential dependence of E_{ads} and E_{int} of Mg(0001) in comparison to Mg(10$\bar{1}$0) and Mg(10$\bar{1}$1). Similar behavior can be seen in Li system. As seen from PES Li(100) has four possible neighboring adatoms, whilst Li(110) only has two (Fig. S4a). Thus, larger change in adsorption and lateral interaction energies with applied potential is observed for Li(100) than for Li(110).

Due to parabolic relation to potential, the change in energy clearly depends on the considered potential region. For a change in potential of 1 V, change in adsorption energy can be anywhere from 0 meV to approximately 200 meV, and change in lateral interaction energy from 0 meV to approximately 150 meV. For the standard working battery regime of −0.2 V/Mg (V/Li) to 0 V/Mg (V/Li), both adsorption energy and interaction energy can be approximated as linearly dependent on potential (Fig. 2b). In this region, for both Mg and Li system, the adsorption energy decreases with decreasing potential, i.e. adatoms become more strongly adsorbed. The slope is about 80 meV/V, 50 meV/V, and 30 meV/V for Mg(0001), Mg(10$\bar{1}$1), and Mg(10$\bar{1}$1), respectively, and 70 meV/V and 15 meV/V for Li(100) and Li(110), respectively. The interaction energy exhibits opposite behavior in this region, and it is increasing with decreasing potential (the adatoms feel weaker interaction between each other) with slope of about −70 meV/V, −30 meV/V, −90 meV/V and −40 meV/V for Mg(0001), Mg(10$\bar{1}$0), Li(100) and Li(110), respectively, whilst it is negligible for Mg(10$\bar{1}$1).

The change in adsorption and interaction energies in the 200 mV wide standard working battery regime is up to approximately 15 meV. Thus, this change will not have a huge impact on the overall dynamics in this narrow potential range. However, if we compare the calculated values for adsorption and interaction energy in the narrow standard working battery regime with their values at potential of zero charge, it is clearly seen that in general the difference can be substantial, up to 60 meV and 140 meV for adsorption and interaction energies, respectively (Fig. 2b). This demonstrates that results obtained with calculations which do not consider proper standard working battery potential (or do not take potential into account at all) provide information about energetics that are possibly not able to describe processes at the standard working battery regime.

Aside from adsorption and lateral interaction energies, potential dependent diffusion barriers were also calculated. In nucleation theory of growth, the diffusion barriers predominately determine the rate of a process and were suggested to serve as a descriptor for dendrite growth [11]. Similarly to adsorption and lateral interaction energies, diffusion barriers also exhibit parabolic dependency on potential. The potential dependence of diffusion barriers in the standard working battery regime is from up to 7 meV for Mg system and up to 4 meV for Li system. Comparing diffusion barriers at the standard working battery regime with the one at PZC demonstrates that the change in diffusion barriers is up to 7 meV and 13 meV for Mg and Li system, respectively. Although these values are low, they correspond to a change of energy barrier of up to 30%. Following Eq. (3), this change in diffusion barrier leads to a change of the k-rate at room temperature of about 1.3 and 1.7 times for Mg and Li, respectively.

Weak potential dependence of diffusion barriers is in accordance with previous theoretical work [10]. It can be rationalized by the delocalized charge on Mg and Li surface, which enables good screening of the electric field on the metal surface as described by the metallicity index developed in another work [30]. In the present case the Li or Mg adatom is strongly mixed with the bulk metal band (Fig. S5) and its interaction with the surface is nearly not affected by the potential change (high metallicity) [30].

3.3. Kinetics of the Mg and Li system and respective relaxation times

To assess the effect of the potential on the morphology evolution, all of the potential dependent energetics have to be considered in the scope of kinetics of the system. This was done using kMC simulations. The results of kMC simulations provide a total energy of the system versus time. The total energy E_{tot} is the sum of adsorption energy E_{ads} for all the adatoms, and interaction energy E_{int} of the pairwise lateral interaction terms. As the number of adatoms on the surface in kMC simulation does not change with time, contribution of adsorption energy is constant. However, due to attractive interaction (negative interaction energy) the E_{tot} decreases during temporal evolution. At times which are much larger than the typical timescale of surface reactions, E_{tot} reaches a plateau, i.e. its local minimum and its quasi-relaxed state. As the

interaction energy is negative, the quasi-relaxed state is in the form of packed morphology.

First plateau typically represents packed morphology of only a couple of atoms. The system stays in that state for a certain time which depends on the energetics of the system. When the coupled adatoms start forming bigger clusters E_{tot} starts decreasing again. Then, the second plateau is reached. This process of smaller clusters forming bigger clusters can repeat itself a couple of times depending on the surface, as seen in the varying number of plateaus for different surfaces (Figs. S3b and S4b). For example, on Mg(10$\bar{1}$1) surface three plateaus can be identified before the system reaches the fourth and final plateau where all adatoms form the biggest possible cluster for that particular surface orientation, i.e. the relaxed state. In comparison, Mg(10$\bar{1}$0) has one plateau before it reaches the relaxed state, whereas Li(100) exhibits only one and final plateau, i.e. goes straight to the relaxed state, without any intermediate quasi-relaxed states. The time at which the system becomes relaxed, i.e. when it reaches the final plateau, is determined as the relaxation time τ.

Surfaces Mg(0001) and Li(110) are specific and require further explanation. Mg(0001) exhibits a couple of plateaus where the adatoms form islands. At approximately 10^{-7} s the morphology is already highly relaxed. However, at approximately 10^{-6} s E_{tot} starts decreasing again (Fig. S3b). After some time, all adatoms on the surface would form one single island, which corresponds to fully relaxed state of Mg(0001). Nevertheless, the quasi-relaxed configuration at approximately 10^{-7} s can be regarded as relaxed, as the tendency for epitaxial growth is evident, and also because in reality the adatoms will never form a single island. The E_{tot} vs. time graph for Li(110) exhibits only one plateau (Fig. S4b). However, in this case it is not the final relaxed state. Instead, it is the first quasi-relaxed state, where only a couple of adatoms are forming packed morphology. Based on the similarity of PESs and on the analysis of configuration at these plateaus, we can regard the plateau observed in Li(110) as equivalent to the first plateau of Mg(10$\bar{1}$0) and Mg(10$\bar{1}$1) (Fig. S3 and S4). With no significant interaction, the Li(110) system has no driving mechanism for the E_{tot} to start decreasing again and to eventually reach the fully relaxed state, and therefore Li(110) remains stranded in this quasi-relaxed state. We cannot speak of true relaxation time for Li(110), but instead define the time when the kMC simulation for Li(110) ended as the lowest estimate of the relaxation time.

Fig. 3 shows the relaxation time τ vs. potential for all studied surfaces (the lowest estimate of the relaxation time for Li(110)). The error bars on the relaxation time values are obtained from running each kMC simulation at least 5 times with the same input parameters, changing only the initial random seed (Figs. S3b and S4b). The results show trends for relaxation times vs. potential, which are in agreement with the potential dependence of adsorption and interaction energies, and diffusion barriers.

For Mg(0001) the relaxation times rise with the potential up to $V \approx 1$ V/Mg, which represent the maximum E_{ads} and minimum E_{int}, and fall above $V \approx 1$ V/Mg. For Mg(10$\bar{1}$0), the trend is similar, except that the turning point is between $V \approx 0.3$ V/Mg and $V \approx 0.9$ V/Mg, where maximum of E_{ads} and minimum of E_{int} are, respectively. For both geometries, the differences are small due to diffusion barrier E_{diff} not being significantly dependent on the potential, as seen in Fig. 2. Finally, for Mg(10$\bar{1}$1), the trend is again parabolic with the turning point slightly above $V \approx 0$ V/Mg, and with much larger differences due to stronger E_{diff} dependency on the potential. Relaxation times are in agreement with our previous results obtained at PZC [19]. However they are slightly larger for Mg(10$\bar{1}$0) and Mg(10$\bar{1}$1) (previously $\tau \approx 10^{-6}$ s and $\tau \approx 10^{-2}$ s, respectively) due to the fact that here the exchange mechanism diffusion is neglected. Although exchange diffusion has a low k-rate and thus occurs rarely, we observed in our previous work that at larger timescales it can still contribute to a faster relaxation, leading to shorter relaxation times.

For Li(100) the relaxation time decreases with the increasing potential, which is likely due to the effect of decreasing E_{diff} with the increasing potential (turning slightly above $V \approx 1.5$ V/Li). This leads to faster diffusion at larger potentials (k-rates are proportional to exp(-E_{diff}) as seen from Eq. (3)) and thus to shorter relaxation times. For Li(110), the longest relaxation time is reached at $V \approx 1$ V/Li.

The surfaces with the highest area fraction to the lowest area fractions in the standard working battery regime are as follow: Mg(10$\bar{1}$1), Mg(10$\bar{1}$0), and Mg(0001) for Mg system, and Li(110) and Li(100) for Li system (Fig. 1). Comparison between diffusion barriers of the most commonly present Mg and Li surface reveals that the barriers are higher for Mg system (0.3 eV vs. 0.05 eV for Mg(10$\bar{1}$1) and Li(110), respectively). This is in contradiction with the proposition that the diffusion barriers can be used as a descriptor for dendrite growth, as it is well-accepted that Li forms dendrites, whilst Mg is less prone to dendrite formation. There are two possible explanations for the contradictory results. First is that the diffusion barriers on their own are not a sufficient descriptor for dendrite growth. The relaxation time of a specific surface depends not solely on the diffusion barrier, but also on the lateral interaction energy. The interaction energy on Mg(10$\bar{1}$1) is approximately four times stronger than on Li(110). As discussed before, due to very low interaction energy Li(110) does not reach fully relaxed state. The first quasi-relaxed state for both Li(110) and Mg(10$\bar{1}$1) is reached after approximately 10^{-9} s, despite of much higher diffusion barrier of Mg(10$\bar{1}$1) (Table 1). The second explanation of the apparently contradictory results is that the studied systems were not modeled in enough detail. The presented study does not consider some of the important processes that are occurring in the realistic system, such as the current rate, roughness of the surface, electrolyte decomposition, surface films building on the anode, etc. On the DFT level the impact of surface roughness can be taken into account by studying diffusion barriers across terraces and stepped surfaces. These diffusion barriers determine how easily a particle propagates to a lower terrace. If this diffusion is hindered by large barriers, the surface will be prone to three-dimensional growth, i.e. dendrite growth is probable. Thus, the diffusion barriers across terraces and stepped surfaces could be a more suitable descriptor for dendrite growth than the herein studied diffusion barriers on smooth surfaces. Furthermore, the current rate could play an important role in morphology evolution. In the kMC simulations we studied surfaces with constant coverage. If the current rate would be taken into account the coverage would increase during deposition. In this case the E_{tot} vs. time plots could exhibit a different behavior and different relaxation times as obtained herein.

4. Conclusion

Herein we present the effect of potential on morphology evolution for most commonly present Mg and Li surfaces. By using the Wulff construction we first show that the crystal shape can be highly dependent on the potential. We find that the surface with the highest area fraction of neutral system is not necessarily the relevant one when it comes to deposition and surface diffusion. To obtain relevant results, it is therefore necessary to define the most commonly present surface at the potential of interest, instead of performing a study on the most stable surface of the neutral system.

Furthermore, results demonstrate that the adsorption and lateral interaction energies as well as diffusion barriers at standard working battery regime differ from their values at potential of zero

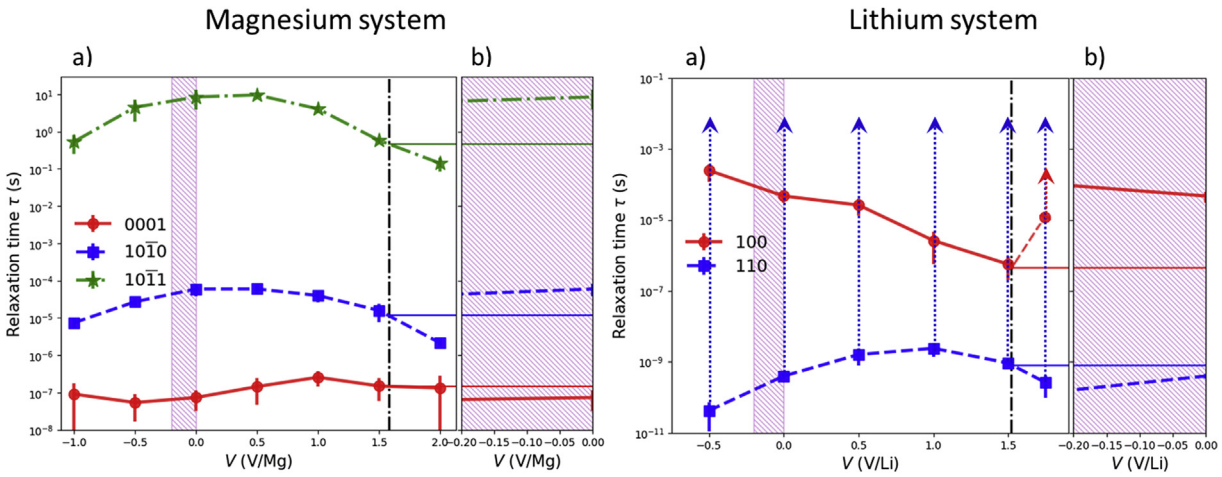

Fig. 3. (left) Potential dependence of relaxation time τ for Mg and (right) potential dependence of relaxation time τ for Li(100), and lowest estimate of relaxation time for Li(110) system. (a) Graphs plotted in a wide potential range. Standard working battery regime is marked with pink shaded region, whereas potential of zero charge (1.58 V/Mg and 1.52 V/Li) is marked with black line. (b) Potential dependent relaxation time τ at standard working battery regime. Solid horizontal red, blue and green line represent values of relaxation time at PZC for Mg(0001), Mg(10$\bar{1}$0), and Mg(10$\bar{1}$1), respectively, in Mg system, and for Li(100) and Li(110) in Li system. Due to negligible lateral interaction energy on Li(100) surface at V = 1.75 V/Li the relaxation is not reached at the time when simulation ended. Thus, the relaxation time for Li(100) at 1.75 V/Li is longer than the lowest limit indicated on the plot. (For interpretation of the references to colour in this figure legend, the reader is referred to the Web version of this article.)

Table 1
Area fractions, diffusion barriers, lateral interaction energies and approximate relaxation times at the standard working battery regime for the studied Mg and Li surfaces in the order of their decreasing area fraction. *For Li(110) the lowest estimate of the relaxation time is given. Due to negligible interaction energy Li(110) is not expected to relax in accessible simulation time.

System	Area fraction (%)	Diffusion barrier E_{diff} (eV)	Lateral interaction energy E_{int} (eV)	Relaxation time τ (s)
Mg(10$\bar{1}$1)	50	0.3	−0.38	1
Mg(10$\bar{1}$0)	25	0.03	−0.32	10^{-4}
Mg(0001)	22	0.02	−0.41	10^{-7}
Li(110)	65	0.05	−0.09	$>10^{-2}$*
Li(100)	30	0.1	−0.2	10^{-4}

charge. Potential dependence of energetics results in diffusion and relaxation time, i.e. the dynamics of the system, being dependent on potential as well. This emphasizes the importance of taking the suitable potential range into account in the calculations.

To investigate the phenomenon of dendritic growth we applied multiscale modeling. The potential dependent results obtained from DFT on the atomistic level were upscaled using kinetic Monte Carlo. From the system dynamics point of view, we calculated the relaxation times for different Li and Mg surfaces. In some systems the potential dependency is very weak (for example, Mg(0001)), while for others, it can lead to over 3 orders of magnitude difference in the relaxation times across the studied potential range (for example, Li(100)). Consequently, this affects the rate of forming packed morphologies on the surface which depends on the surface type and on the potential.

It has been suggested that diffusion barriers can be used as descriptor for dendrite growth. However, we find that diffusion barrier on the most commonly present Mg surface at standard working battery regime is six times higher than the one on the most commonly present Li surface under the same conditions. Using the assumption that diffusion barriers can be used as a descriptor for dendrite growth, this would suggest that Mg is more prone to dendrite growth than Li. Based on this we conclude that either the diffusion barriers are not a sufficient descriptor for dendrite growth, or that the studied systems are too simplified. The relaxation time depends also on lateral interaction energies and surface coverage, and some of the important processes that are occurring in the realistic systems (current rate, roughness of the surface, decomposition products, etc.) are not taken into account in the present study. The first step to a more realistic system is to consider the roughness of the surface by studying the diffusion barriers across terraces and stepped surfaces. This is the topic of future work. Furthermore, the obtained DFT results can be used in meso and macro scale simulations, where in addition the current rate, solid-electrolyte interphase, and electrolyte dynamics could be taken into account. All of this can have substantial impact on morphology evolution.

Although the results of the work presented herein are obtained on a simplified system, they demonstrate the importance of studying the system at the standard working battery regime and taking potential dependence into account. Herein, previously developed Grand canonical DFT approach was aptly applied to study energetics and dynamics of various surfaces at different potentials. To the best of our knowledge, such a study has not yet been done. The approach is computationally affordable, transferable, widely applicable, and can be used in most of the periodic DFT codes. Therefore, this approach offers an accessible way of tackling an intrinsic multiscale problem such as the morphology evolution at chosen potentials, and presents a valuable tool for the communities dealing with batteries, catalysts, and electrochemistry in general.

Declaration of competing interest

The authors declare that they have no known competing financial interests or personal relationships that could have

appeared to influence the work reported in this paper.

Acknowledgements

AKL and DK gratefully acknowledge the support of Slovenian Research Agency (research project J2-8167, research core funding P2-0393, P1-0044, and P2-0152) and Honda R&D Europe (Germany). AH and JSF thank the French National Research Agency for its support through the Labex STORE-EX project (ANR-10LABX-76-01). Part of this work was supported by EU through the POROUS4APP project (H2020-NMP-PILOTS-2015n n°686163). Discussion with Robert Dominko and Jan Bitenc are gratefully acknowledged. This work was performed using HPC resources from GENCI-CINES (Grant 2019-A0060910369).

Appendix A. Supplementary data

Supplementary data to this article can be found online at https://doi.org/10.1016/j.electacta.2020.136493.

References

[1] D. Linden, T.B. Reddy, Handbook of Batteries, 2002, https://doi.org/10.1002/9780470933886.ch1.
[2] H. Tavassol, M.K.Y. Chan, M.G. Catarello, J. Greeley, D.G. Cahill, A.A. Gewirtha, Surface coverage and SEI induced electrochemical surface stress changes during Li deposition in a model system for Li-ion battery anodes, J. Electrochem. Soc. 160 (6) (2013) 888–896, https://doi.org/10.1149/2.068306jes.
[3] M.M. Thackeray, C. Wolverton, E.D. Isaacs, Electrical energy storage for transportation - approaching the limits of, and going beyond, lithium-ion batteries, Energy Environ. Sci. 5 (7) (2012) 7854–7863, https://doi.org/10.1039/c2ee21892e.
[4] J.B. Goodenough, Rechargeable batteries: challenges old and new, J. Solid State Electrochem. 16 (6) (2012) 2019–2029, https://doi.org/10.1007/s10008-012-1751-2.
[5] X. Cheng, R. Zhang, C. Zhao, Q. Zhang, Toward safe lithium metal anode in rechargeable Batteries : a review, Chem. Rev. 117 (2017) 10403–10473, https://doi.org/10.1021/acs.chemrev.7b00115.
[6] R. Mohtadi, F. Mizuno, Magnesium batteries: current state of the art, issues and future perspectives, Beilstein J. Nanotechnol. 5 (2014) 1291–1311, https://doi.org/10.3762/bjnano.5.143.
[7] J. Muldoon, C.B. Bucur, A.G. Oliver, T. Sugimoto, M. Matsui, H.S. Kim, G.D. Allred, J. Zajicek, Y. Kotani, Electrolyte roadblocks to a magnesium rechargeable battery, Energy Environ. Sci. 5 (3) (2012) 5941–5950, https://doi.org/10.1039/c2ee03029b.
[8] H.D. Yoo, I. Shterenberg, Y. Gofer, G. Gershinsky, N. Pour, D. Aurbach, Mg rechargeable batteries: an on-going challenge, Energy Environ. Sci. 6 (8) (2013) 2265–2279, https://doi.org/10.1039/c3ee40871j.
[9] J. Muldoon, C.B. Bucur, T. Gregory, Quest for nonaqueous multivalent secondary Batteries : magnesium and beyond, Chem. Rev. 114 (2014) 11683–11720, https://doi.org/10.1021/cr500049y.
[10] M. Jäckle, A. Groß, Influence of electric fields on metal self-diffusion barriers and its consequences on dendrite growth in batteries, J. Chem. Phys. 151 (23) (2019), https://doi.org/10.1063/1.5133429.
[11] M. Jäckle, K. Helmbrecht, M. Smits, D. Stottmeister, A. Groß, Self-diffusion Barriers : possible descriptors for dendrite growth in batteries? Energy Environ. Sci. 11 (2018) 3400–3407, https://doi.org/10.1039/c8ee01448e.
[12] M. Jäckle, A. Groß, Microscopic properties of lithium , sodium , and magnesium battery anode materials related to possible dendrite growth related to possible dendrite growth, J. Chem. Phys. 141 (2014) 174710, https://doi.org/10.1063/1.4901055.
[13] C. Ling, D. Banerjee, M. Matsui, Study of the electrochemical deposition of Mg in the atomic level: why it prefers the non-dendritic morphology, Electrochim. Acta 76 (2012) 270–274, https://doi.org/10.1016/j.electacta.2012.05.001.
[14] Q.S. Zhao, Y.N. Nuli, Y.S. Guo, J. Yang, J.L. Wang, Reversibility of electrochemical magnesium deposition from tetrahydrofuran solutions containing pyrrolidinyl magnesium halide, Electrochim. Acta 56 (18) (2011) 6530–6535, https://doi.org/10.1016/j.electacta.2011.04.114.
[15] D. Aurbach, Y. Cohen, M. Moshkovich, The study of reversible magnesium deposition by in situ scanning tunneling microscopy, Electrochem. Solid State Lett. 4 (8) (2002) A113, https://doi.org/10.1149/1.1379828.
[16] M.S. Ding, T. Diemant, R.J. Behm, S. Passerini, G.A. Giffin, Dendrite growth in Mg metal cells containing Mg(TFSI)2/Glyme electrolytes, J. Electrochem. Soc. 165 (10) (2018) A1983–A1990, https://doi.org/10.1149/2.1471809jes.
[17] R. Davidson, A. Verma, D. Santos, F. Hao, C. Fincher, S. Xiang, J. Van Buskirk, K. Xie, M. Pharr, P.P. Mukherjee, et al., formation of magnesium dendrites during electrodeposition, ACS Energy Lett. 4 (2) (2019) 375–376, https://doi.org/10.1021/acsenergylett.8b02470.
[18] J. Bitenc, K. Pirnat, E. Žagar, A. Randon-Vitanova, R. Dominko, Effect of salts on the electrochemical performance of Mg metal–organic battery, J. Power Sources 430 (2019) 90–94, https://doi.org/10.1016/j.jpowsour.2019.04.114.
[19] A. Kopač Lautar, D. Kopač, T. Rejec, T. Bančič, R. Dominko, Morphology evolution of magnesium Facets : DFT and KMC simulations, Phys. Chem. Chem. Phys. 21 (2019) 2434–2442, https://doi.org/10.1039/c8cp06171h.
[20] H. Brune, Microscopic view of epitaxial metal growth: nucleation and aggregation, Surf. Sci. Rep. 31 (4–6) (1998) 125–229, https://doi.org/10.1016/S0167-5729(99)80001-6.
[21] J.A. Venables, Nucleation calculations in a pair-binding model, Phys. Rev. B 36 (8) (1987) 4153–4162, https://doi.org/10.1103/PhysRevB.36.4153.
[22] G.X.X.Y. Wulff, Zur frage der geschwindigkeit Des wachs-, Z. für Kristallogr. - Cryst. Mater. 34 (1901) 449–530, https://doi.org/10.1524/zkri.1901.34.1.449.
[23] R. Tran, Z. Xu, B. Radhakrishnan, D. Winston, W. Sun, K.A. Persson, S.P. Ong, Surface energies of elemental crystals, Sci. Data 3 (2016) 160080, https://doi.org/10.1038/cgt.2016.38.
[24] R. Tran, X. Li, J.H. Montoya, D. Winston, K.A. Persson, Anisotropic work function of elemental crystals, Surf. Sci. 687 (May) (2019) 48–55, https://doi.org/10.1016/j.susc.2019.05.002.
[25] F. Faglioni, B.V. Merinov, W.A.G. Iii, Room-temperature lithium phases from density functional theory, J. Phys. Chem. C 120 (2016) 27104–27108, https://doi.org/10.1021/acs.jpcc.6b08168.
[26] J.-S. Filhol, M. Neurock, Elucidation of the electrochemical activation of water over Pd by first principles, Angew. Chem. Int. Ed. 45 (3) (2006) 402–406, https://doi.org/10.1002/anie.200502540.
[27] M. Mamatkulov, J.S. Filhol, An ab initio study of electrochemical vs. Electromechanical properties: the case of CO adsorbed on a Pt(111) surface, Phys. Chem. Chem. Phys. 13 (17) (2011) 7675–7684, https://doi.org/10.1039/c0cp01444c.
[28] N. Lespes, J. Filhol, Surface science using the electrochemical dimension to build water/Ru(0001) phase diagram, Surf. Sci. 631 (2015) 8–16, https://doi.org/10.1016/j.susc.2014.06.017.
[29] N. Lespes, J.S. Filhol, Using implicit solvent in ab initio electrochemical modeling: investigating Li^+/Li electrochemistry at a Li/solvent interface, J. Chem. Theor. Comput. 11 (7) (2015) 3375–3382, https://doi.org/10.1021/acs.jctc.5b00170.
[30] A. Kopač Lautar, A. Hagopian, J.-S. Filhol, Modeling interfacial Electrochemistry : concepts and tools, Phys. Chem. Chem. Phys. (2020), https://doi.org/10.1039/C9CP06684E.
[31] A. Kopač Lautar, J. Bitenc, T. Rejec, R. Dominko, J.-S. Filhol, M.-L. Doublet, Electrolyte reactivity in the Double layer in Mg Batteries : an interface potential-dependent DFT study electrolyte reactivity in the Double layer in Mg Batteries : an interface potential-dependent DFT study, J. Am. Chem. Soc. (2020), https://doi.org/10.1021/jacs.9b12474.
[32] G. Kresse, J. Furthmüller, Efficiency of ab-initio total energy calculations for metals and semiconductors using a plane-wave basis set, Comput. Mater. Sci. 6 (1) (1996) 15–50, https://doi.org/10.1016/0927-0256(96)00008-0.
[33] G. Kresse, J. Furthmüller, Efficient iterative schemes for ab initio total-energy calculations using a plane-wave basis set, Phys. Rev. B 54 (16) (1996) 11169–11186, https://doi.org/10.1103/PhysRevB.54.11169.
[34] G. Kresse, D. Joubert, From ultrasoft pseudopotentials to the projector augmented-wave method, Phys. Rev. B 59 (3) (1999) 1758–1775, https://doi.org/10.1103/PhysRevB.59.1758.
[35] J.P. Perdew, K. Burke, M. Ernzerhof, Generalized gradient approximation made simple, Phys. Rev. Lett. 77 (18) (1996) 3865–3868, https://doi.org/10.1103/PhysRevLett.77.3865.
[36] K. Mathew, R. Sundararaman, K. Letchowrth-Weaver, T.A. Arias, R.G. Henning, Implicit solvation model for density-functional study of nanocrystal surfaces and reaction pathways, J. Chem. Phys. 8 (2014), 084106, https://doi.org/10.1063/1.4865107.
[37] M. Fishman, H.L. Zhuang, K. Mathew, W. Dirschka, R.G. Hennig, Accuracy of exchange-correlation functionals and effect of solvation on the surface energy of copper, Phys. Rev. B 87 (24) (2013) 245402, https://doi.org/10.1103/PhysRevB.87.245402.
[38] K. Momma, F. Izumi, VESTA 3 for three-dimensional visualization of crystal, volumetric and morphology data, J. Appl. Crystallogr. 44 (6) (2011) 1272–1276, https://doi.org/10.1107/S0021889811038970.
[39] G. Henkelman, B.P. Uberuaga, H. Jónsson, Climbing image nudged elastic band method for finding saddle points and minimum energy paths, J. Chem. Phys. 113 (22) (2000) 9901–9904, https://doi.org/10.1063/1.1329672.
[40] V.G. Dubrovskii, Nucleation Theory and Growth of Nanostructures, Springer, 2014, https://doi.org/10.1007/978-3-642-39660-1.
[41] A.F. Voter, Introduction to the Kinetic Monte Carlo Method, vols. 1–23, 2007.
[42] M.A. Quiroga, A.A. Franco, A multi-paradigm computational model of materials electrochemical reactivity for energy conversion and storage, J. Electrochem. Soc. 162 (7) (2015) 73–83, https://doi.org/10.1149/2.1011506jes.
[43] M. Stamatakis, D.G. Vlachos, A graph-theoretical kinetic Monte Carlo framework for on-lattice chemical kinetics, J. Chem. Phys. 134 (21) (2011) 214115, https://doi.org/10.1063/1.3596751.
[44] J. Nielsen, M. D'Avezac, J. Hetherington, M. Stamatakis, Parallel kinetic Monte Carlo simulation framework incorporating accurate models of adsorbate lateral interactions, J. Chem. Phys. 139 (2013) 224706, https://doi.org/

10.1063/1.4840395.
[45] M. Gabers, J. Bitenc, K. Pirnat, T. Banc, A. Randon-vitanova, R. Dominko, Anthraquinone-based polymer as cathode in rechargeable magnesium batteries, ChemSusChem 8 (2015) 4128–4132, https://doi.org/10.1002/cssc.201500910.
[46] P. Bai, J. Li, F.R. Brushett, M.Z. Bazant, Transition of lithium growth mechanisms in liquid electrolytes, Energy Environ. Sci. 9 (2016) 3221–3229, https://doi.org/10.1039/c6ee01674j.
[47] J. Steiger, Mechanisms of dendrite growth in lithium metal batteries. https://doi.org/10.5445/IR/1000045310, 2015.
[48] J.S. Filhol, M.L. Doublet, Conceptual surface electrochemistry and new redox descriptors, J. Phys. Chem. C 118 (2014) 19023–19031, https://doi.org/10.1021/jp502296p.